NeuroImage 44 (2009) 1304–1311

Contents lists available at ScienceDirect

NeuroImage

journal homepage: www.elsevier.com/locate/ynimg

Hybrid FMT–CT imaging of amyloid-β plaques in a murine Alzheimer's disease model

Damon Hyde [a,c,*], Ruben de Kleine [a], Sarah A. MacLaurin [b], Eric Miller [d], Dana H. Brooks [c], Thomas Krucker [b], Vasilis Ntziachristos [a,e]

[a] Laboratory for Bio-optics and Molecular Imaging, Center for Molecular Imaging Research, Massachusetts General Hospital and Harvard Medical School, Charlestown, MA 02129, USA
[b] Novartis Institutes for Biomedical Research, Global Imaging Group, Cambridge, MA 02139, USA
[c] Electrical and Computer Engineering Dept., Northeastern University, Boston, MA, USA
[d] Electrical and Computer Engineering Dept., Tufts University, Medford, MA, USA
[e] Institute for Biological and Medical Imaging, Technical University of Munich and Helmholtz Center Munich, Munich, Germany

ARTICLE INFO

Article history:
Received 28 August 2008
Revised 15 October 2008
Accepted 21 October 2008
Available online 7 November 2008

ABSTRACT

The need to study molecular and functional parameters of Alzheimer's disease progression in animal models has led to the development of disease-specific fluorescent markers. However, curved optical interfaces and a highly heterogeneous internal structure make quantitative fluorescence imaging of the murine brain a particularly challenging tomographic problem. We investigated the integration of X-ray computed tomography (CT) information into a state-of-the-art fluorescence molecular tomography (FMT) scheme and establish that the dual-modality approach is essential for high fidelity reconstructions of distributed fluorescence within the murine brain, as compared to conventional fluorescence tomography. We employ this method *in vivo* using a fluorescent oxazine dye to quantify amyloid-β plaque burden in transgenic APP23 mice modeling Alzheimer's disease. Multi-modal imaging allows for accurate signal localization and correlation of *in vivo* findings to *ex vivo* studies. The results point to FMT–CT as an essential tool for *in vivo* study of neurodegenerative disease in animal models and potentially humans.

Introduction

Longer human lifespan brings an increased prevalence of age related conditions such as neurodegenerative diseases (Ferri et al., 2005). Among these, Alzheimer's disease (AD) is the primary cause of neuronal degradation, accounting for between 42 and 81% of dementia cases. From an average onset of 80 years, AD incidence increases exponentially, with more than 50% of 90–95 year old individuals likely being symptomatic (Nussbaum and Ellis, 2003). Furthermore, most similarly aged asymptomatic individuals are likely to acquire at least some amyloid-β plaques and hyperphosphorylated tau (tangles) which are the primary pathological hallmarks of the disease (Goedert and Spillantini, 2006).

The widespread prevalence and significant impact upon both patients and families have spurred the development of investigational tools for *in vivo* evaluation of both disease progression and the efficacy of potential therapeutic strategies. In the laboratory, several lines of transgenic animals exhibiting altered expression levels of amyloid precursor protein (APP) have been developed using mutations similar to those seen in early-onset familial AD (FAD) (Chishti et al., 2001; Hsiao et al., 1996; Games et al., 1995; Sturchler-Pierrat et al., 1997). In particular, the APP23 line contains a mutated human APP gene that results in a 7-fold over-expression of APP compared to control animals (Sturchler-Pierrat et al., 1997), leading to the formation of amyloid plaques with age correlated increasing proliferation. Additionally, these mice show all other pathological hallmarks of Alzheimer's disease such as hyperphosphorylated tau and manifest learning and memory deficits. Since their development, these animals have been widely used in research ranging from disease pathogenesis (Sturchler-Pierrat and Staufenbiel, 2000) to behavioral research (Prut et al., 2007) and imaging of altered brain vasculature (Krucker et al., 2004; Beckmann et al., 2003; Meyer et al., 2008).

Linked to the development of appropriate animal models for understanding and finding treatments for AD is the search for appropriate methods that can non-invasively image AD biomarkers *in vivo*. *In vivo* longitudinal imaging offers real time evaluation of drug efficacy and has been linked to accelerating therapeutic discovery. In response, imaging techniques such as positron emission tomography (PET) and magnetic resonance imaging (MRI) have been applied to AD visualization. Fluorodeoxyglucose (FDG) PET studies have examined AD related aberrations in glucose metabolism (Hammoud et al., 2007), while other radiotracers such as FDDNP (Agdeppa et al., 2001, 2004) and Pittsburgh Compound-B (Small et al., 2006; Rowe et al., 2007) can directly assess amyloid plaque burden and tau bundles. Structural alterations such as decreased

* Corresponding author.
E-mail addresses: dhyde@ece.neu.edu (D. Hyde), v.ntziachristos@tum.de (V. Ntziachristos).

1053-8119/$ – see front matter © 2008 Elsevier Inc. All rights reserved.
doi:10.1016/j.neuroimage.2008.10.038

gray matter volume (Good et al., 2001) and altered vasculature (Krucker et al., 2004) have been imaged using magnetic resonance. Developments in fluorescence probes have yielded the ability to target amyloid-β plaques using the AO1987 probe (Hintersteiner et al., 2005). Given the choice, fluorescence methods have advantages for biological research as they offer versatility that overcomes several of the technical difficulties of other modalities such as the use of ionizing radiation and the requirement for dedicated cyclotron facilities to produce adept PET probes or challenges in visualizing molecular function with MRI. However current optical methods offer inadequate imaging performance. Fluorescence microscopy lacks the ability to penetrate deeper than a few hundred microns, preventing non-invasive imaging of the brain. Planar fluorescence imaging, previously utilized (Hintersteiner et al., 2005), offers single projection viewing and compromised accuracy due to the strong non-linear dependence of fluorescence intensity on activity depth and tissue optical properties. Furthermore, current state-of-the-art fluorescence tomography methods, developed to improve on planar imaging by using theoretical models of photon propagation in tissues, do not have adequate resolving power to produce accurate brain images. This is a particular problem when determining distributed fluorescence activity, i.e. spatially extended fluorescence patterns, as expected in neurodegenerative disease. Indeed, we demonstrate here that conventional fluorescence molecular tomography (FMT) of distributed fluorescence activity in the animal head is particularly challenging due to the optically heterogeneous structures and highly curving boundary characteristic of this problem.

In this work we developed a tomographic dual-modality X-ray CT/FMT method which significantly improved imaging performance in the mouse head by incorporating structural information from X-ray CT images into the FMT inversion problem. The use of image priors from an anatomic modality has been suggested as a technique to improve diffusive optical tomography (Boas and Dale, 2005; Brooksby et al., 2003, 2005; Guven et al., 2005; Li et al., 2003; Schweiger and Arridge, 1999; Lin et al., 2007; Davis et al., 2007; Gulsen et al., 2006; Intes et al., 2004; Ntziachristos et al., 2002). These approaches typically make assumptions on the relationship between tissue structures and optical properties, and have been shown to work well in spectroscopic problems of tissue absorption and scattering using simulated data (Boas and Dale, 2005). *In vivo,* the use of *a priori* information has been employed to the measurement of oxy- and deoxy-hemoglobin and other tissue chromophores in the human breast (Brooksby et al., 2005). By contrast, making assumptions about the *in vivo* distribution of exogenous fluorescent probes is significantly more challenging, as their spatial distribution need not be correlated with anatomic structure. For this reason, we discuss here a method suitable for *in vivo* measurements that does not make rigid assumptions concerning the relation of fluorescence bio-distribution and the CT anatomical structures. Instead it uses *a priori* information derived from X-ray CT to first construct improved diffusion models using the finite element method (FEM) as the basis of a new two-step inversion technique. The first of these steps uses structural information to define an adaptive reduced-dimensional problem which computes an appropriate penalty term for each region based on the experimentally collected fluorescence measurements, which is then applied in the second step. In this manner this approach makes no specific prior assumptions on fluorescence bio-distribution and allows the collected data to be the primary driving force in the reconstructions, not user-defined restrictions as typical in previous implementations derived for *in vivo* use. We use this technique to showcase the previously undocumented capacity for the use of anatomical priors for *in vivo* fluorescence tomography. Our reconstructions indicate that the multi-modal approach provides a high degree of both structural and quantitative correlation with *ex vivo* imaging studies, and is essential for the accurate visualization of neurodegenerative biomarkers *in vivo*.

Methods

Tomographic imaging

Fluorescence imaging was performed using a state-of-the-art 4th generation fluorescence molecular tomography system based on the multi-angle collection of transmission data in a free-space geometry. A 650-nm wavelength continuous wave diode laser (B&W Tek, Newark DE) was used for illumination, with x–y scanning performed by a set of two linear translation stages (Velmex, Bloomfield NY). Transillumination images were collected using a charge coupled device (CCD) camera (VersArray 512b, 512×512 resolution, Roper Scientific, Trenton NJ), cooled to −35 °C for noise reduction.

Images were collected with the laser located at each point in a 3 column, 5 row grid of size 0.6 cm by 1.4 cm. Camera and translation stage control were implemented using Winview (Roper Scientific, Trenton NJ) and a custom Matlab (The Mathworks, Natick MA) interface. Excitation wavelength measurements were collected using a bandpass filter (Three-cavity interference, 652±9.5 nm, Andover, Salem MA). Fluorescence measurements used a combination of a bandpass (three-cavity interference at 710±10 nm, Andover, Salem MA) and a longpass filter (Cutoff 695 nm; Omega Optical, Brattleboro VT) for wavelength selection.

All measurements employed for tomographic inversion used the normalized Born ratio to correct for optical inhomogeneities within the mouse head. This normalization technique divides each fluorescence measurement by its corresponding excitation measurement, thereby eliminating the need to explicitly solve the full system of coupled differential equations (Ntziachristos and Weissleder, 2001; Soubret et al., 2005). Additionally, the Born ratio provides significant robustness to inhomogeneities within the animal, and negates the need to determine source and detector coupling coefficients, among other unknown constants (Soubret et al., 2005). To provide surface structural information, a final set of data was collected, consisting of silhouette images at an increased number of projection angles. All post processing and image reconstruction algorithms were implemented in Matlab.

Surface reconstruction and registration

Localization of the animal surface was achieved using a previously described volume carving algorithm (Lasser et al., 2008; Deliolanis et al., 2007). An electroluminescent plate was placed behind the animal to allow the CCD to collect silhouette images from a large number of angles. The volume carving algorithm employs this information to extract the location of the animal's surface within the imaging chamber. This allows for both proper mathematical modeling of photon diffusion and correct mathematical projection of source and detector patterns onto the surface.

Internal structural prior information was provided by a X-ray CT data set, collected from a C57BL/6 mouse using an X-SPECT small animal imaging system. (Gamma Medica, Northridge, CA). The data were analyzed and manually segmented to differentiate brain matter from surrounding bone and soft tissue. The software package AMIRA (Mercury Computer Systems Inc., Chelmsford MA) was used to apply an affine transform to co-register an isosurface representing the air–tissue interface in the CT data with the surface information obtained from the FMT system. The transform matrix, along with a version of the CT segmentation label map, downsampled to 128^3 voxels, was exported to Matlab for use in both the forward and inverse aspects of the FMT imaging problem. This allowed individual reconstruction voxels to be labeled with a tissue type using a nearest neighbor interpolation approach.

Multi-modality imaging

Subsequent integration into the FMT inversion algorithm was done by including a Tikhonov-type regularization term L in the minimization equation:

$$x = \underset{x}{\operatorname{argmin}} ||u - f(x)||_2^2 + \lambda ||\mathbf{L}x||_2^2$$

where x is the image to be determined, u is the collected data, and $f(x)$ is the forward operator relating the image to the data. λ is a parameter controlling the degree of regularization, and is selected by use of L-Curve analysis (Hansen, 1992). Here, **L** is a diagonal matrix whose individual values are determined by the tissue labels given to the associated voxels in x. Determination of these values is done by obtaining a parameterized inverse solution given an assumption of a constant value across the entire region. Solution of the above minimization was computed using an approximate maximum likelihood approach based on the statistics of the normalized data (Hyde et al., 2007).

In vivo imaging

Two hours prior to imaging, each mouse was injected with a 1 mg/kg dose of AO1987 (Novartis Institutes for BioMedical Research Inc.) by tail vein injection. Additionally, each animal's head was shaved and a depilatory cream applied to ensure good coupling between the laser and tissue. Immediately prior to imaging, animals were anesthetized by tail vein injection of ketamine (100 mg/kg, Boehringer Ingelhein, St. Joseph MO) and xylazine (10 mg/kg, Bedford Laboratories, Bedford OH). This was supplemented as necessary during imaging by additional intraperitoneally injected doses. Animals were mounted vertically within the chamber, with their abdomen and lower extremities restrained within a cylindrical tube. To properly orient and restrain the head, the animal's incisor teeth were fastened to the top of the rotation stage with suture thread. Imaging sessions lasted approximately 1 hour from initial anesthetization to completion and euthanasia by CO_2 inhalation. All imaging was performed according to procedures approved by the Massachusetts General Hospital Review Board.

Mean FMT data signal

Collected FMT data was used to generate images approximating those collected *in vivo* with uniform illumination planar transmission systems. A single projection was selected, corresponding to the CCD camera being positioned directly over the dorsal surface of the head. Laser source locations were on the ventral side. Images from fluorescence and excitation channels were summed across all source locations to yield single images for each channel. The normalized Born ratio was then applied to correct for differences in excitation intensity. Mean normalized intensity over the brain region was then computed, for comparison with *in vivo* tomographic reconstructions and *ex vivo* planar imaging results.

Ex vivo imaging

Immediately following *in vivo* FMT imaging, each animal was perfused intra-aortically with a 4% paraformaldehyde in phosphate buffered saline (PBS) solution to fix and solidify brain tissue. Brains were surgically extracted and imaged whole using a planar reflectance imaging system before being manually sliced into 8 axial sections, approximately 1.5 mm thick, for further examination. Illumination for planar reflectance imaging was with the same 650 nm continuous wave diode laser used in the FMT system. Beam expanders enabled a planar illumination field, rather than the point illumination used for tomographic imaging. Data was collected at excitation and emission wavelengths using the same wavelength selection filters as the FMT system, as well as under white room light. Post-processing using ImageJ and Matlab (The Mathworks, Natick MA) was used to identify the cortical region of each slice and compute the mean normalized fluorescence signal using the Born ratio.

Confocal imaging

Fixed brain slices were mounted onto CoverWell & Secure Seal Imaging Chambers (Electron Microscopy Sciences, Harfield, PA) with Crystal Mouse (BioMeda, Foster City CA). Photographs of each slice were taken with an Olympus C7070 Digital Camera mounted to an Olympus Model SZX12 Research Stereo Microscope. Regions of interest were selected on these images to guide region selection for confocal microscopy. Confocal microscopy data was collected with a Zeiss LSM 510 Meta confocal microscope with the two photon (NLO) feature from a subset of these regions. Confocal images were acquired using the 635 nm HeNe laser. The emitted light was collected through a 650–710 nm bandpass filter. A 10 layer stack was collected of each field then collapsed to one maximum projection image. Data were analyzed using the CRi Maestro (CRi, Woburn, MA) measurement software to select plaques (defined as pixel clusters above certain threshold values); the sum of the selected plaques (area in pixels) was then normalized within that image.

Results

Multi-modal FMT–CT imaging

All tomographic animal imaging was performed using a recently developed state-of-the-art FMT system employing a free space geometry and full angular data collection in transmission mode (Fig. 1) (Deliolanis et al., 2007). This system allows for use of arbitrary source-laser and detector point patterns on the surface of the animal. Collection of photon propagation data from multiple angles increases the information content of the signal and allows for improvements in spatial resolution and quantification. Localization of the animal surface was done using multiple silhouette images and a previously described volume carving algorithm (Lasser et al., 2008).

X-ray CT was performed on a X-SPECT micro-CT scanner (Gamma Medica, Northridge, CA). The data were analyzed and manually segmented to differentiate brain and cortical regions, bone and soft tissue (Fig. 2). An affine transform to co-register the surface computed by the FMT system with an isosurface from the CT image representing the air–tissue interface was implemented using the software package AMIRA (Mercury Computer Systems Inc., Chelmsford MA). This linear map aligned the FMT and CT coordinate systems, allowing the structural information to be used in both the forward and inverse aspects of the resulting tomography problem. For the forward problem, i.e. a theoretical prediction of photon propagation in tissue, finite element method (FEM) solutions to the diffusion approximation were computed within a head geometry constructed from the CT structural information. The sensitivity functions resulting from this computation were used to construct a first order Born model of light propagation.

The inverse problem, determining an unknown fluorescence distribution from measured data, was implemented by preferentially regularizing voxels based on an adaptive two step method that assigns regularization values based on information contained in the acquired dual wavelength measurements. The first step uses a subdivision of the three classically segmented tissue types (i.e. brain, cortex, soft tissue) to improve discrimination between regions and break possible symmetries in the inversion problem (Fig. 2a). This improved the numerical properties of the problem and resulted in significantly more stable results. The non-cortical brain was divided into left and right hemispheres, while the cortical region was broken into dorsal,

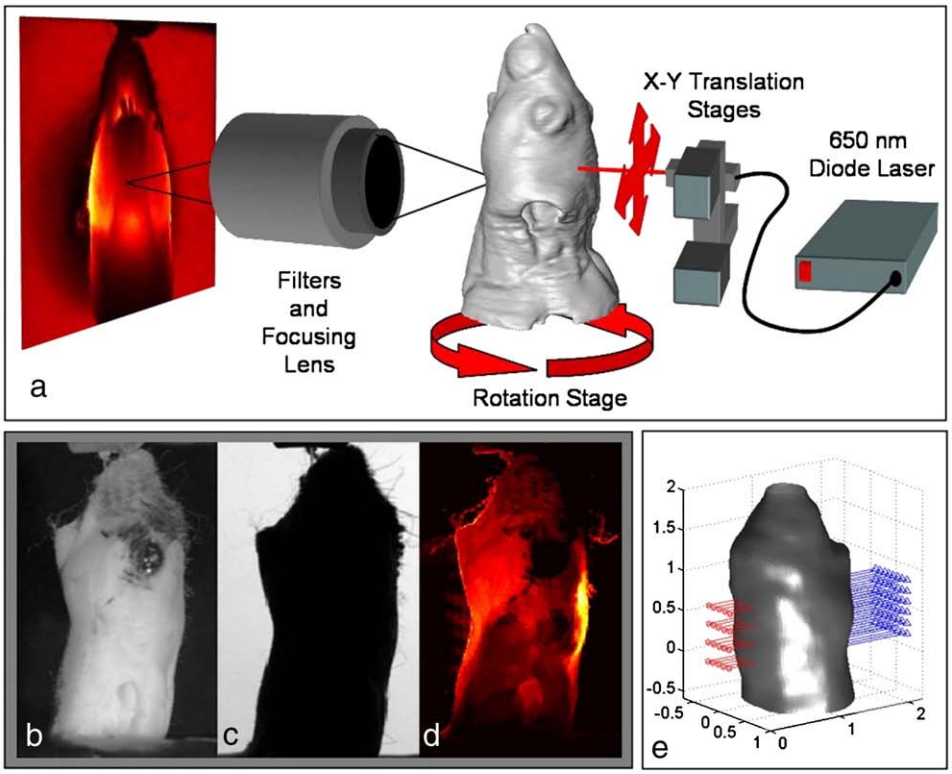

Fig. 1. Data collection and localization of animal surface. (a) Schematic of data collection system. Source fiber driven by a 650 nm diode laser was mounted on translation stages for focusing and localization on animal surface. Collection of data was done in a transmission geometry using an electrically cooled CCD camera and appropriate filters for wavelength selection. A representative excitation channel image is shown. (b) White light image of mouse head. (c) Corresponding silhouette image used for surface localization. 360 such images were used for the surface generation algorithm. (d) Summation of normalized (fluorescence/excitation) data across all source locations for this projection angle. (e) Resolved surface location, showing source (red) and detector (blue) patterns mathematically projected onto surface for a single projection angle.

left, and right lateral segments. All non-brain tissues are treated as a single type for simplicity and to prevent introduction of artifacts into the solutions. While the selection of subdivided areas was empirical here, we are currently investigating analytical methods to offer quantitative subdivision guidance. This segmentation was incorporated into an approximate maximum likelihood solution (Hyde et al., 2007) as an additive penalty term, with relative weights based on an initial solution of a low dimensional parameterized problem which assumed a piecewise constant basis defined by the subdivisions. Essentially, this step accurately determines the strength of fluorescence in each of the subdivisions by inverting a low parametric and easily solved problem. The determination of the piece-wise subdivision-specific fluorescence strengths was employed to scale corresponding regularization parameters. The importance of this step is that the prior information on fluorescence strength is implemented based on the information contained in the collected data, i.e. not by user-dependent selection.

The performance of the developed multi-modal technique was done using simulated data generated on a geometry derived from X-ray CT animal measurements, prior to *in vivo* application. The geometry was identical to that employed experimentally, but the lack of model error allowed the establishment of a best-case baseline and examination of effects specific to the inversion technique (Fig. 3). Even under these ideal simulated conditions, the reconstruction of cortical fluorescence yielded poor images without the use of structural prior information. Due to the spatial distribution of the cortex and non-uniqueness of the inverse problem, the reconstructions showed a fluorescing mass located centrally within the brain, rather than peripherally in the cortex. Furthermore, the images without prior information were corrupted by surface artifacts arising from high model sensitivities near the sources and detectors causing over fitting of noise in the data. The use of structural priors eliminated these artifacts and provided results which much more accurately reflected the original fluorescence distribution.

In vivo imaging

Six mice were imaged during the course of this study: four APP23 tg mice, at ages 17 to 28 months, and two APP23 wt control mice, ages 13 and 17 months. For all APP23 tg mice, the initial parameterized inversion identified one or more of the cortical segments as the region (s) most likely to contain fluorescence, a conclusion consistent with prior expectations. By contrast, applying an initial inversion step to the wt mouse shown in Fig. 5 did not identify strong fluorescence within any individual region. This resulted in a reconstruction with a less structured fluorescence distribution and lower overall intensity, suggesting that activity may be the result of free fluorochrome or non-specific binding. Full resolution reconstructions of the APP23 tg mice in our algorithm's second step resulted in images showing fluorescence activity primarily within the cortical region of the brain.

Images constructed using our structurally guided multi-modal algorithm consistently showed a marked improvement in quality and significant decrease in artifacts compared to those regularized using standard Tikhonov regularization with the identity matrix. As in the simulated tests, without structural prior information reconstructions of *in vivo* data were dominated by diffuse fluorescent masses and surface artifacts, offering little qualitative or quantitative information about plaque localization. The developed multi-modal algorithm eliminated these artifacts and enabled quantitative measurement of fluorochrome concentrations which were correlated with measurements gathered *ex vivo* by other imaging methods detailed below.

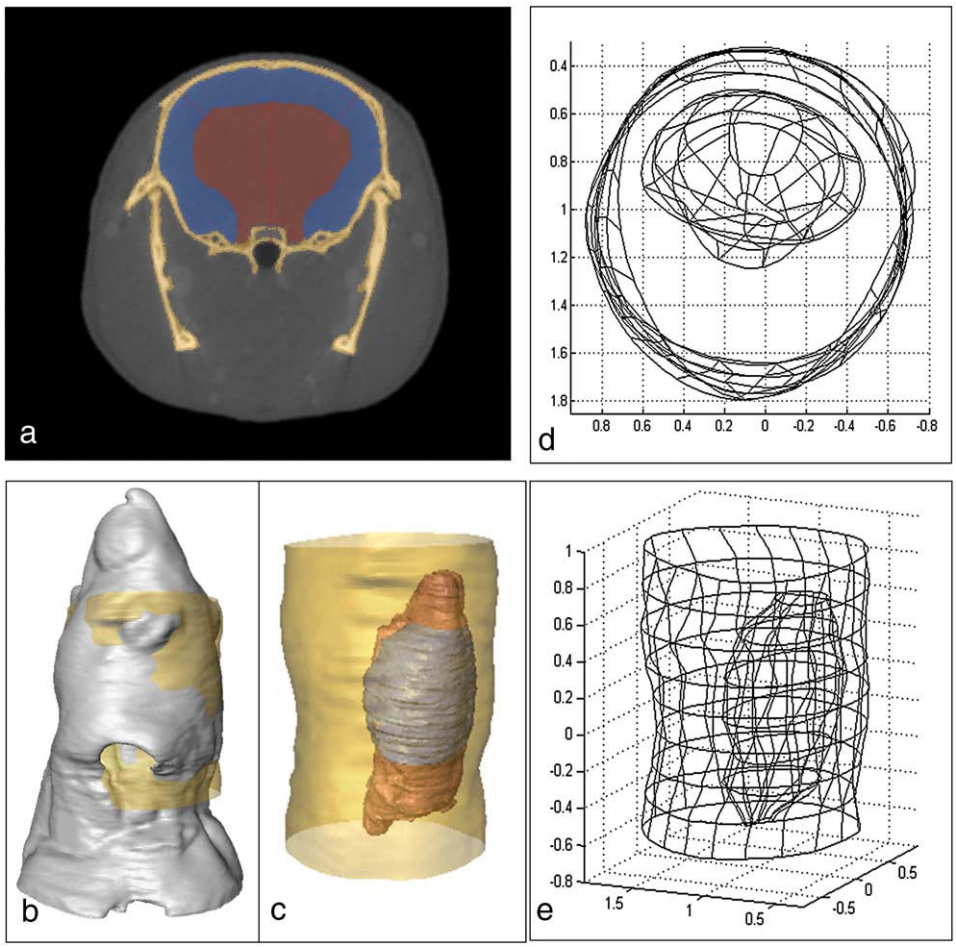

Fig. 2. CT–FMT registration and modeling geometry. (a) A 2D slice of the CT data, showing labeled brain (red) and cortical (blue) regions. Dotted red lines indicate where regions were subdivided prior to the inversion process. (b) An isosurface from the CT image (gray) superimposed with surface computed by FMT volume carving algorithm (yellow). This alignment allows for use of CT information in the FMT problem. (c) Alignment between modalities allows the brain (red) and cortical (blue) regions to be appropriately located within the surface computed by the FMT system (yellow). (d–e) Contour information was extracted from the segmentation information and used to construct surface meshes prior to generation of a tetrahedral mesh for obtaining solutions to the diffusion equation using the finite element method (FEM).

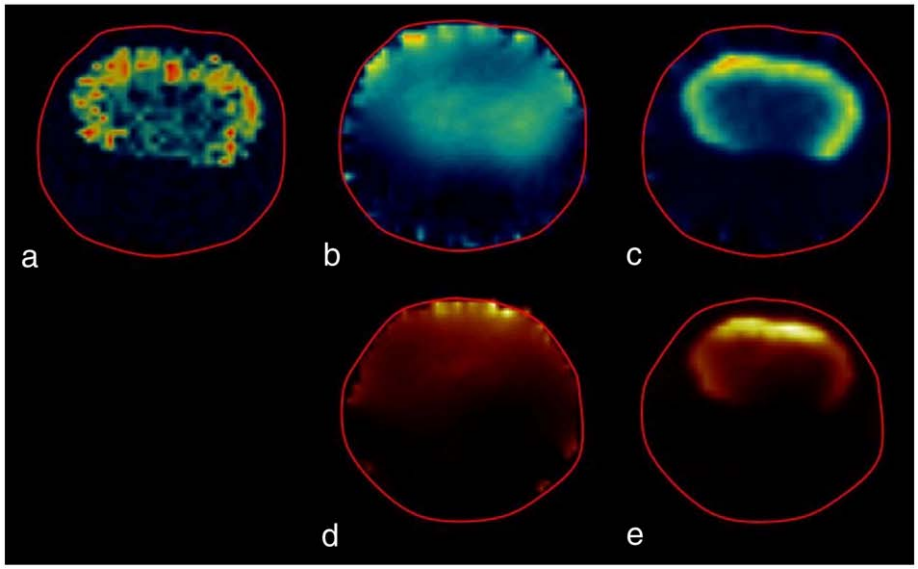

Fig. 3. FMT reconstructions with/without structural *a priori* information: (a–c) simulated imaging results. (a) Synthetic image created for data generation. Image pixels within each anatomical region were generated as instances of independent, identically distributed Gaussian processes. (b) FMT reconstruction using data generated from (a), without the use of prior structural information. (c) Reconstruction incorporating *a priori* knowledge of tissue region boundaries. (d–e) FMT imaging results for a 28 month APP23 tg mouse 2 hours after injection with 1 mg/kg of AO1987. (d) Reconstruction using standard regularization techniques. (e) Reconstruction incorporating structural *a priori* knowledge.

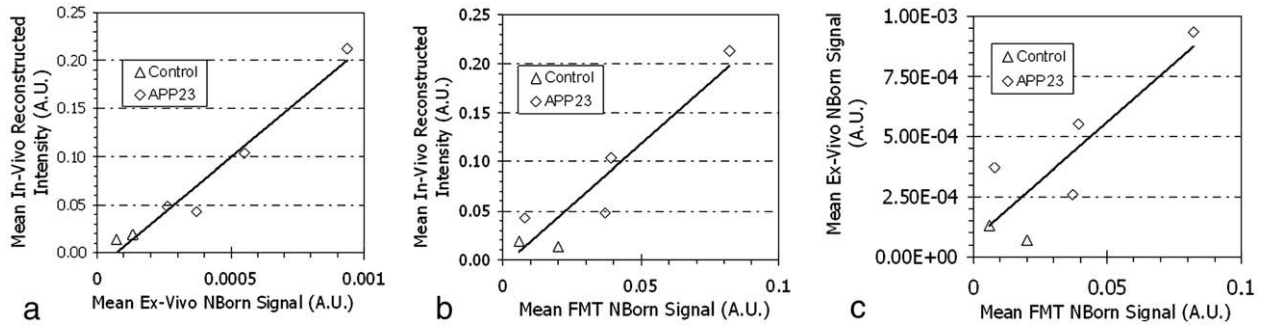

Fig. 4. *In-vivo* vs *ex-vivo* correlation. (a) Correlation between *in vivo* reconstructed activity and normalized fluorescence intensity measured *ex vivo* (x-axis) (R^2=0.9587). (b) Comparison of mean input FMT data for a single projection (x-axis) with resulting FMT reconstructed intensity (R^2=0.7422). The single projection was chosen with the camera positioned directly above the dorsal side of the head. (c) Mean input FMT signal (x-axis) as in (b), correlated with measured *ex vivo* fluorescence activity (R^2=0.8712).

Correlative ex vivo imaging

Immediately following *in vivo* imaging, each animal was euthanized and its brain surgically excised for imaging with a planar fluorescence reflectance system. Individual image slices were analyzed to determine mean normalized fluorescence intensity levels within the manually segmented cortex. The resulting values were then plotted against the mean *in vivo* reconstructed cortical intensity from the FMT system (Fig. 4) yielding a highly linear relationship (R^2=0.9587) between the signal observed by *ex vivo* imaging and multi-modal FMT reconstructed intensities. By contrast, the mean FMT input signal from a single projection, which approximates planar transmission imaging, shows a markedly lower correlation with the *ex vivo* measurements (R^2=0.7422). While correlation between mean FMT input signal and reconstructed values is observed (R^2=0.8712), it is lower than that present between *ex vivo* data and reconstructed values. Additionally, higher input values do not always yield higher reconstructed intensities, indicating that the tomographic process is properly correcting for variations in geometry and fluorochrome localization within the head.

Subjective evaluation of the *ex vivo* images further confirms the relationship between underlying activity and the FMT reconstructions (Fig. 5). No lesions are seen in the C57BL/6 control mouse, while varying degrees of plaque density appear in the cortex of the APP23 tg

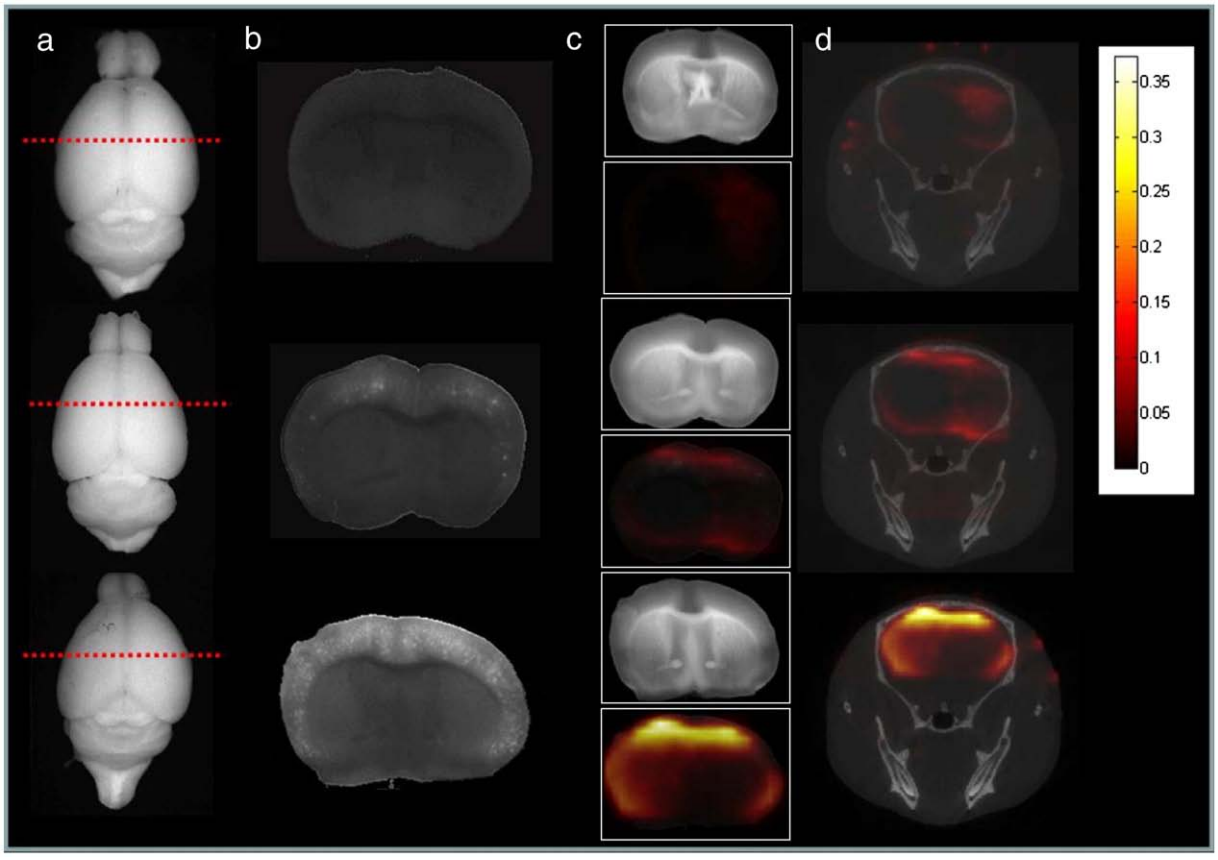

Fig. 5. *Ex vivo* versus *in vivo* FMT imaging comparison for 13 month old C57B/6 control mouse (first row) a 17 month old APP23 tg mouse (Second row) and a 26 month old APP23 tg mouse (third row). (a) The first column shows full brain images in the excitation channel using a planar reflectance imaging system. The red dotted line denotes the approximate location corresponding to the slice shown in subsequent columns. (b) Planar reflectance images of normalized fluorescence from a single slice are then presented in the second column. (c) The third column presents planar images at the excitation wavelength (top) and FMT reconstructions overlaid on normalized planar fluorescence images (bottom). (d) *In vivo* multi-modal FMT reconstructions are shown in the final column for a slice corresponding to the same location as the *ex vivo* images, overlaid on a representative CT slice. All FMT reconstructions are scaled to the same colorbar.

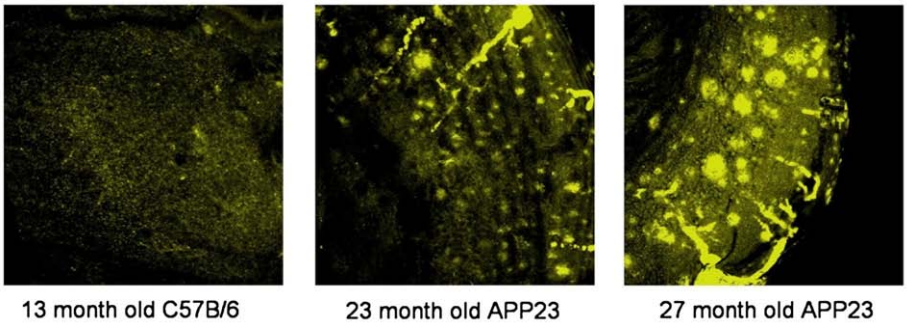

Fig. 6. Representative confocal images of thick brain slices from a 13 month old C57B/6 mouse and two APP23 transgenic mice, at ages 23 and 27 months. In each image, amyloid-β plaques appear as bright areas.

mice. Fluorescence localization in the FMT images correlates well with these *ex vivo* findings. While the resolution of the FMT system cannot resolve the individual lesions seen in the planar fluorescence images, the pattern of plaque deposits in the planar images correlates well with that seen in the FMT reconstructions.

Further validation of both the AO1987 probe and the multi-modal FMT–CT imaging technique were provided by confocal microscopic imaging of the excised brain slices. Confocal images of cortical and hippocampal brain regions showed dense plaque accumulations in the APP23 tg mice, while the images from control mice were void of all staining (Fig. 6). Thick slices were analyzed to quantify the total area within cortex and hippocampus occupied by amyloid-β plaques. The average fractional area for five APP23 mice (average age 23.6 months) was 11.62% (SEM 0.22) while control wt mice lacked any measurable signal. This was in accordance to previously established plaque load in these mice (Sturchler-Pierrat and Staufenbiel, 2000). Notably larger blood vessels in the cortical area stained positive.

Discussion

Non-invasive fluorescence tomography of laboratory animals can become a natural extension of *in vitro* fluorescence assays and microscopy studies given that high image fidelity and quantification accuracy can be achieved *in vivo*. Fluorescence is an essential modality in biological research and the extension of fluorescence imaging resonates with the biology culture. In addition, fluorescence imaging offers attractive characteristics such as the ability to simultaneously differentiate multiple markers based on multi-spectral imaging (Han et al., 2001), the use of non-ionizing radiation and the widespread use of fluorescent proteins (Giepmans et al., 2006), recently also extending to the near-infrared (Merzlyak et al., 2007; Shu et al., 2006; Shcherbo et al., 2007). The use of appropriate scrambled or inactive probes emitting in a different wavelength compares to the active probe, can further generate imaging protocols where each mouse serves as its own control, for example by independently resolving probe binding vs. probe bio-distribution, leading to increased accuracy and minimization of the animals required to obtain statistically significant results. While *in vivo* imaging does not replace traditional *ex vivo* studies or intravital microscopy measurements based on established microscopy protocols, it can be used to provide volumetric data at the tissue level and accurately guide the selection of animals for entering established high resolution imaging protocols for deciphering events at the cellular and subcellular level.

For these reasons, several methodologies have been described for quantitative fluorescence imaging of tissue. However none of these methods have proven so far sufficient for *in vivo* imaging of neurodegenerative disease. The particular challenge associated with optical imaging of neurodegenerative diseases is that the disease is rarely confined within a small volume of the brain but it is more typical that a distributed spread pattern arises in the brain. Therefore, while localized cancer-related fluorescence activity has been resolved with conventional fluorescence tomography in the animal brain (Ntziachristos et al., 2002), this technology has difficulty accurately visualizing distributed fluorescence bio-distributions as shown here with relevant simulations and *in vivo*.

We demonstrated here that a hybrid method based on state-of-the-art FMT measurement combined with CT structural information enables the *in vivo* visualization of plaque distributions in a mouse model for Alzheimer's disease. We show that the use of this technique is essential to produce highly accurate fluorescence images, in contrast to using standard tomographic methods. This capability provides an important new tool for *in vivo* imaging of Alzheimer's disease progression within a single mouse, and suggests applicability to imaging other neurodegenerative diseases in the murine head. The information obtained from such studies could provide real time evaluation of the efficacy of new anti-amyloid treatments and insights into Alzheimer's disease pathology over time. By utilizing the same method at several spectral windows, with corresponding fluorochromes or expressed fluorescent proteins from transgenic animals emitting at different spectral bands, different disease biomarkers and signaling pathways or cellular migration can be visualized including physiological and molecular markers.

An important aspect of the method developed is the restriction of the use of *a priori* information to the definition of physical regions in the head; i.e. without other restrictions on fluorescence bio-distribution. This allows the use of CT structural information in a manner which does not overly impose itself onto the fluorescence reconstruction. Instead, the collected FMT measurements themselves are allowed to determine the final output. This is important because operator bias and/or conceptions of a desired output can strongly impact the resulting reconstructions when using *a priori* information in a more rigid form, especially in fluorescence mode where the underlying spatial distribution does not necessarily correlate with anatomic structure, and thus the information required to make such assumptions is unavailable.

One drawback seen in the images from several of the mice with heavier cortical amyloid-β plaque loads was a degree of spatially non-uniform sensitivity to the presence of fluorochrome. Lesions present in the dorsal portion of the cortex are more easily reconstructed than those present in the left and right lateral segments, and result in higher reconstructed intensities than the lateral segments. This can be explained by the geometry of the head, differences in absorption between the brain and surrounding tissue, and the presence of esophageal and ear canal void spaces within the head. In particular, the void spaces alter photon transport in a manner not accounted for by a diffusion model. Ongoing research into more complex physical models and improvements to data collection methodologies will both help to alleviate these shortcomings.

The method developed herein describes a co-registration scheme that can use X-ray CT images acquired at a different time-point compared to the fluorescence measurements. Using advanced processing schemes, this concept could also be adapted to using mouse atlases instead of actual scans. However, the most obvious, and perhaps important, extension to this work will be the development of a single physical system for the collection of both FMT and CT data sets. As presented here, registration between the two is available only because the skull structure of each mouse presents a relatively straightforward rigid transformation, where the internal spatial relationships are maintained regardless of animal orientation or soft tissue distortion. Data collected concurrently or under identical placement could eliminate these image registration issues, enabling more accurate performance and the potential extension of the methods to areas other than the animal head, for example the chest cavity and abdomen, enabling the use of multi-modal FMT for preclinical imaging of virtually any fluorescent target. Even in its present form however, the method developed could complement stand-alone free-space FMT systems and offer a significantly higher degree of performance.

In conclusion, multi-modal fluorescence imaging of tissue offers the potential for significant improvements in image fidelity and *in vivo* quantification over conventional fluorescence tomography methods. With the advent of new probe technologies and transgenic platforms utilizing fluorescence proteins, one could envision multi-modal FMT used to perform rapid and high-throughput visualization of neurodegenerative biomarkers. Optical sampling of human brain parameters has also been showcased in several studies (Villringer and Chance, 1997; Tanner et al., 2005), further pointing to the possibility for clinical propagation of the technology presented here. While it is not foreseen that the entire human brain can be visualized with optical methods in clinical settings, it would be nevertheless feasible to probe cortex biomarkers at depths up to 3–5 cm, which could be sufficient for obtaining diagnostic information or clinical information on therapeutic efficacy.

Acknowledgment

We thank Akos Szilvasi (NIBRI), for his technical help with the confocal microscopy.

References

Agdeppa, E.D., Kepe, V., Liu, J., et al., 2001. Binding characteristics of radiofluorinated 6-dialkylamino-2-naphthylethylidene derivatives as positron emission tomography imaging probes for beta-amyloid plaques in Alzheimer's disease. J. Neurosci. 21 art. no.-RC189.

Agdeppa, E.D., Kepe, V., Shoghi-Jadid, K., et al., 2004. 2-Dialkylamino-6-acylmalononitrile substituted naphthalenes (DDNP analogs): novel diagnostic and therapeutic tools in Alzheimer's disease (vol. 5, pg 404, 2003). Mol. Imaging Biol. 6, 68.

Beckmann, N., Schuler, A., Mueggler, T., et al., 2003. Age-dependent cerebrovascular abnormalities and blood flow disturbances in APP23 mice modeling Alzheimer's disease. J. Neurosci. 23, 8453–8459.

Boas, D.A., Dale, A.M., 2005. Simulation study of magnetic resonance imaging-guided cortically constrained diffuse optical tomography of human brain function. Appl. Opt. 44, 1957–1968.

Brooksby, B.A., Dehghani, H., Pogue, B.W., Paulsen, K.D., 2003. Near-infrared (NIR) tomography breast image reconstruction with a priori structural information from MRI: algorithm development for reconstructing heterogeneities. IEEE J. Sel. Top. Quantum Electron. 9, 199–209.

Brooksby, B., Jiang, S.D., Dehghani, H., et al., 2005. Combining near-infrared tomography and magnetic resonance imaging to study in vivo breast tissue: implementation of a Laplacian-type regularization to incorporate magnetic resonance structure. J. Biomed. Opt. 10 (5), 1504.

Chishti, M.A., Yang, D.S., Janus, C., et al., 2001. Early-onset amyloid deposition and cognitive deficits in transgenic mice expressing a double mutant form of amyloid precursor protein 695. J. Biol. Chem. 276, 21562–21570.

Davis, S.C., Dehghani, H., Wang, J., et al., 2007. Image-guided diffuse optical fluorescence tomography implemented with Laplacian-type regularization. Opt. Express 15, 4066–4082.

Deliolanis, N., Lasser, T., Hyde, D., et al., 2007. Free-space fluorescence molecular tomography utilizing 360° geometry projections. Opt. Lett. 32, 382–384.

Ferri, C.P., Prince, M., Brayne, C., et al., 2005. Global prevalence of dementia: a Delphi consensus study. Lancet 366, 2112–2117.

Games, D., Adams, D., Alessandrini, R., et al., 1995. Alzheimer-type neuropathology in transgenic mice overexpressing V717f beta-amyloid precursor protein. Nature 373, 523–527.

Giepmans, B.N.G., Adams, S.R., Ellisman, M.H., Tsien, R.Y., 2006. Review — the fluorescent toolbox for assessing protein location and function. Science 312, 217–224.

Goedert, M., Spillantini, M.G., 2006. A century of Alzheimer's disease. Science 314, 777–781.

Good, C.D., Johnsrude, I.S., Ashburner, J., et al., 2001. A voxel-based morphometric study of ageing in 465 normal adult human brains. Neuroimage 14, 21–36.

Gulsen, G., Birgul, O., Unlu, M.B., et al., 2006. Combined diffuse optical tomography (DOT) and MRI system for cancer imaging in small animals. Technol. Cancer Res. Treat. 5, 351–363.

Guven, M., Yazici, B., Intes, X., Chance, B., 2005. Diffuse optical tomography with a priori anatomical information. Phys. Med. Biol. 50, 2837–2858.

Hammoud, D.A., Hoffman, J.M., Pomper, M.G., 2007. Molecular neuroimaging: from conventional to emerging technique. Radiology 245, 21–42.

Han, M.Y., Gao, X.H., Su, J.Z., Nie, S., 2001. Quantum-dot-tagged microbeads for multiplexed optical coding of biomolecules. Nat. Biotechnol. 19, 631–635.

Hansen, P.C., 1992. Analysis of Discrete Ill-posed problems by means of the L-Curve. SIAM Rev. 34, 561–580.

Hintersteiner, M., Enz, A., Frey, P., et al., 2005. In vivo detection of amyloid-beta deposits by near-infrared imaging using an oxazine-derivative probe. Nat. Biotechnol. 23, 577–583.

Hsiao, K., Chapman, P., Nilsen, S., et al., 1996. Correlative memory deficits, A beta elevation, and amyloid plaques in transgenic mice. Science 274, 99–102.

Hyde, D., Miller, E., Brooks, D.H., Ntziachristos, V., 2007. A statistical approach to inverting the Born ratio. IEEE Trans. Med. Imag. 26, 893–905.

Intes, X., Maloux, C., Guven, M., et al., 2004. Diffuse optical tomography with physiological and spatial a priori constraints. Phys. Med. Biol. 49, N155–N163.

Krucker, T., Schuler, A., Meyer, E.P., et al., 2004. Magnetic resonance angiography and vascular corrosion casting as tools in biomedical research: application to transgenic mice modeling Alzheimer's disease. Neurol. Res. 26, 507–516.

Lasser, T., Soubret, A., Ripoll, J., Ntziachristos, V., 2008. Surface reconstruction for free-space 360 degrees fluorescence molecular tomography and the effects of animal motion. IEEE Trans. Med. Imag. 27, 188–194.

Li, A., Miller, E.L., Kilmer, M.E., et al., 2003. Tomographic optical breast imaging guided by three-dimensional mammography. Appl. Opt. 42, 5181–5190.

Lin, Y., Gao, H., Nalcioglu, O., Gulsen, G., 2007. Fluorescence diffuse optical tomography with functional and anatomical a priori information: feasibility study. Phys. Med. Biol. 52, 5569–5585.

Merzlyak, E.M., Goedhart, J., Shcherbo, D., et al., 2007. Bright monomeric red fluorescent protein with an extended fluorescence lifetime. Nat. Med. 4, 555–557.

Meyer, E.P., Ulmann-Schuler, A., Staufenbiel, M., Krucker, T., 2008. Altered morphology and 3D architecture of brain vasculature in a mouse model for Alzheimer's disease. Proc. Natl. Acad. Sci. U. S. A. 105, 3587–3592.

Ntziachristos, V., Weissleder, R., 2001. Experimental three-dimensional fluorescence reconstruction of diffuse media by use of a normalized Born approximation. Opt. Lett. 26, 893–895.

Ntziachristos, V., Tung, C.H., Bremer, C., Weissleder, R., 2002. Fluorescence molecular tomography resolves protease activity in vivo. Nat. Med. 8, 757–761.

Ntziachristos, V., Yodh, A.G., Schnall, M.D., Chance, B., 2002. MRI-guided diffuse optical spectroscopy of malignant and benign breast lesions. Neoplasia 4, 347–354.

Nussbaum, R.L., Ellis, C.E., 2003. Genomic medicine: Alzheimer's disease and Parkinson's disease. N. Engl. J. Med. 348, 1356–1364.

Prut, L., Abramowski, D., Krucker, T., et al., 2007. Aged APP23 mice show a delay in switching to the use of a strategy in the Barnes maze. Behav. Brain Res. 179, 107–110.

Rowe, C.C., Ng, S., Ackermann, U., et al., 2007. Imaging beta-amyloid burden in aging and dementia. Neurology 68, 1718–1725.

Schweiger, M., Arridge, S.R., 1999. Optical tomographic reconstruction in a complex head model using a priori region boundary information. Phys. Med. Biol. 44, 2703–2721.

Shcherbo, D., Merzlyak, E.M., Chepurnykh, T.V., et al., 2007. Bright far-red fluorescent protein for whole-body imaging. Nat. Med. 4, 741–746.

Shu, X.K., Shaner, N.C., Yarbrough, C.A., et al., 2006. Novel chromophores and buried charges control color in mFruits. Biochemistry 45, 9639–9647.

Small, G.W., Kepe, V., Ercoli, L.M., et al., 2006. PET of brain amyloid and tau in mild cognitive impairment. N. Engl. J. Med. 355, 2652–2663.

Soubret, A., Ripoll, J., Ntziachristos, V., 2005. Accuracy of fluorescent tomography in the presence of heterogeneities: study of the normalized born ratio. IEEE Trans. Med. Imag. 24, 1377–1386.

Sturchler-Pierrat, C., Staufenbiel, M., 2000. Pathogenic mechanisms of Alzheimer's disease analyzed in the APP23 transgenic mouse model. Ann. N. Y. Acad. Sci. 920, 134–139.

Sturchler-Pierrat, C., Abramowski, D., Duke, M., et al., 1997. Two amyloid precursor protein transgenic mouse models with Alzheimer disease-like pathology. Proc. Natl. Acad. Sci. U. S. A. 94, 13287–13292.

Tanner, K., D'Amico, E., Kaczmarowski, A., et al., 2005. Spectrally resolved neurophotonics: a case report of hemodynamics and vascular components in the mammalian brain. J. Biomed. Opt. 10 (6), 4009.

Villringer, A., Chance, B., 1997. Non-invasive optical spectroscopy and imaging of human brain function. Trends Neurosci. 20, 435–442.